DOI: 10.19884/j.1672-5220.202305003

Modification of Graphite Carbon Nitride by Nitrogen-Doping and in situ Loading $CoSe_x$ as Co-Catalyst by Light-Assisted Synthesis for Enhanced Photocatalytic Hydrogen Production

LIU Siwei[1,2], XI Chuanjun[1,2], ZHANG Linping[1,2], XUAN Weimin[1,2], HOU Yu[1,2*]
1. College of Chemistry and Chemical Engineering, Donghua University, Shanghai 201620, China
2. Key Laboratory of Science and Technology of Eco-Textile, Ministry of Education, Donghua University, Shanghai 201620, China

Abstract: Developing an efficient photocatalyst for hydrogen production is crucial for the conversion of solar energy to hydrogen. An efficient photocatalytic hydrogen evolution material was prepared by altering the graphite carbon nitride (CN) through nitrogen-doping and employing $CoSe_x$ as a co-catalyst through a photochemical synthesis route. The optimal photocatalytic performance of the material is 285 times higher than that of CN. Photoelectrochemical experiments demonstrate that nitrogen-doping and introducing $CoSe_x$ can effectively promote the separation of photogenerated charge carriers, thus increasing the hydrogen evolution activity of CN. This work may provide new perspectives for the preparation of novel photocatalysts by photochemical deposition methods.

Key words: photocatalyst; $CoSe_x$; co-catalyst; hydrogen production; nitrogen-doping
CLC number: O644.1 **Document code**: A
Article ID: 1672-5220(2024)03-0249-08

Open Science Identity (OSID)

0 Introduction

In recent years, energy shortage and environmental deterioration have become two major problems that hinder the development of society[1-5]. Most of the energy that we are consuming is from fossil fuels with inadequate reserves. Combustion of non-renewable energy could lead to global warming, acid rain and other air pollution phenomena, which severely affect the environment[6-8]. Therefore, developing clean and renewable energy is of great importance. Hydrogen energy has the advantages of high combustion value (120–142 MJ/kg) and production of zero pollution[9], so it is a potential alternative to replace fossil energy. Among all the hydrogen production ways, photocatalytic hydrogen production from solar energy has been viewed as an ideal route since solar energy is inexhaustible[10-11].

Photocatalytic hydrogen production by utilizing semiconductors has received great attention since Fujishima et al.[12] reported that TiO_2 had the capability of splitting water photoelectrochemically. In the last several years, different kinds of semiconductors, such as TiO_2[13-14], ZnO[15-16], CdS[17-18] and $ZnIn_2S_4$[19-20], were extensively investigated for photocatalytic water splitting. Apart from these inorganic semiconductors, organic semiconductors were also applied for water splitting, among which graphite carbon nitride (CN) has become a star material due to its non-toxic, low-cost, excellent stability and special electronic structure[21-23]. However, the limited light absorption and the rapid recombination of photogenerated charge carriers limit its application in photocatalytic hydrogen production[24-26]. These shortcomings of CN can be overcome by adopting several strategies, including element doping[27-28], morphology control[26-29], combining with co-catalysts[30-32] and other semiconductors[33-34], etc.

Among these methods, combining with co-catalysts is conductive to accelerate the migration of interfacial electrons, and element doping can adjust the band gap, thus improving the light absorption[35-36]. Loading co-catalysts can be achieved by photochemical synthesis, which is operated under mild operating conditions. The co-catalyst prepared by this method could be in the amorphous phase and located at the site of electron transfer, which is more conducive to the proton reduction reaction[37-38]. Yu et al.[39] successfully anchored amorphous Ni-P alloy particles onto CN by photodeposition and the obtained photocatalyst improved hydrogen activity. Transition metal selenides can serve as co-catalysts since they have relatively low electrical resistance, which facilitates electron transport. In addition, selenium atoms with large radius and low

Received date: 2023-05-12
Foundation item: National Natural Science Foundation of China (No. 21872025)
* Correspondence should be addressed to HOU Yu, email: houyu@dhu.edu.cn
Citation: LIU S W, XI C J, ZHANG L P, et al. Modification of graphite carbon nitride by nitrogen-doping and in situ loading $CoSe_x$ as co-catalyst by light-assisted synthesis for enhanced photocatalytic hydrogen production[J]. *Journal of Donghua University (English Edition)*, 2024, 41(3): 249-256.

electronegativity usually weakly bind to the outer electrons of transition metals, which is favorable to the redox reaction. The common transition metal selenide co-catalysts include $NiSe_2$, $CoSe_2$, $MoSe_2$ and so on.

Based on the above, a novel photocatalyst was designed by coupling nitrogen-doped CN (N-CN) with $CoSe_x$ through the light-assisted synthesis. The photocatalytic hydrogen production activity of the prepared composite photocatalyst would be superior to that of CN and N-CN. The results of photoelectrochemical characterization showed a more efficient separation between photogenerated electrons and holes during the photocatalytic process, which would contribute to the enhanced hydrogen performance.

1 Materials and Methods

1.1 Materials

The purity of all the chemical reagents is analytical grade and no further purification is required during use. Sodium selenite (Na_2SeO_3) and cobalt nitrate hexahydrate ($Co(NO_3)_2 \cdot 6H_2O$) were purchased from Shanghai Adamas Reagent Co., Ltd., China. Citric acid monohydrate, triethanolamine (TEOA) and other chemicals were purchased from Sinopharm Group, China.

1.2 Synthesis

1.2.1 Synthesis of CN and N-CN

Citric acid monohydrate (10 mg) was grounded and mixed well with urea (10 g) in a mortar, and then the mixture was transferred to a crucible which was put in a muffle furnace and calcined at 550 ℃ for 4 h (2.5 ℃/min). After cooling to room temperature, nitrogen-doped CN was obtained, noted as N-CN. CN was prepared by a similar method, with the exception that citric acid monohydrate was not added.

1.2.2 Synthesis of $CoSe_x$-loaded N-CN (N-CN-$CoSe_x$)

N-CN-$CoSe_x$ was synthesized through an in situ photochemical synthesis method, which involved loading $CoSe_x$ onto N-CN. N-CN (50 mg) was grounded for 10 min and transferred to a beaker. Then 0.1 mol/L $Co(NO_3)_2 \cdot 6H_2O$ (1.02 mL) and 0.1 mol/L Na_2SeO_3 (1.53 mL) were added. After that, the mixture was stirred for 1 h and transferred to a reactor. The reaction temperature was controlled at 10 ℃ by circulating cold water. After degassing for 30 min, a 300 W xenon lamp was switched on for 30 min, and then the product was collected, washed with deionized water, and dried at 50 ℃ for 6 h in a vacuum oven. By changing the amounts of Na_2SeO_3 and $Co(NO_3)_2 \cdot 6H_2O$, photocatalysts with different $CoSe_x$ loadings were prepared (denoted as N-CN-$CoSe_x$-1, N-CN-$CoSe_x$-2, N-CN-$CoSe_x$-3 and N-CN-$CoSe_x$-4), as shown in Table 1. CN-$CoSe_x$-3 was also prepared by a similar method for comparison, except that CN was used instead of N-CN.

Table 1 Synthesis of N-CN-$CoSe_x$

Sample	Volume of Na_2SeO_3 solution /mL	Volume of $Co(NO_3)_2 \cdot 6H_2O$ solution /mL
N-CN-$CoSe_x$-1	0.13	0.08
N-CN-$CoSe_x$-2	0.51	0.34
N-CN-$CoSe_x$-3	1.53	1.02
N-CN-$CoSe_x$-4	2.30	1.53
CN-$CoSe_x$-3	1.53	1.02

1.3 Measurement and characterization

1.3.1 Structure, morphology and composition characterization

In this paper, X-ray diffraction (XRD) was employed to analyze the phase composition and structure of the catalyst. Energy dispersive X-ray spectroscopy (EDX) was used to determine the molar fraction of Co and Se in the catalyst. X-ray photoelectron spectroscopy (XPS) was used to analyze the elemental composition and valence states of the catalyst. Field-emission scanning electron microscopy (FESEM) was used to observe the microscopic surface morphology of the catalyst. Transmission electron microscopy (TEM) was used to characterize the microscopic morphology and elemental distribution of the catalyst. UV-Vis diffuse reflectance spectroscopy was employed to analyze the absorption range of the catalyst and estimate the bandgap width of the catalyst, and the accessories used for testing were integrating spheres, with a wavelength range of 200 to 800 nm.

1.3.2 Photocatalytic hydrogen production measurement

Labsolar-III AG photocatalytic analysis system (Beijing Perfectlight Technology Co., Ltd., Beijing, China) was used to evaluate the photocatalytic hydrogen production performance of the samples. In a typical experiment, 20 mg sample was dispersed in 100 mL aqueous solution containing 10 mL TEOA and 90 mL deionized water in a 250 mL reactor. Xenon lamp (300 W, Beijing Perfectligh Technology Co., Ltd., Beijing, China) was the light source for driving photocatalytic reactions. Before light irradiation, the system was degassed for 30 min, and the solution temperature was kept at 10 ℃ by circulating cold water. The amount of producted hydrogen was detected by gas chromatography with a thermal conductivity detector (GC 7900, Techcomp Instrument Limited, Shanghai, China; carrier gas: Ar).

1.3.3 Photoelectrochemical characterization

The photoelectrochemical characterizations, such as electrochemical impedance spectroscopy (EIS, the real part of the impedance Z'' is plotted against the imaginary part of the impedance Z') and transient photocurrent intensity response (*I-t* curve), were carried out in a standard three-electrode system. The reference electrode and the counter electrode were Ag/AgCl electrode and platinum wire electrode, respectively. The working

electrode was prepared by pipetting 100 μL liquid (a mixture of 5 mg catalyst, 100 μL Nafion (a trade name of a perfluorosulfonic acid polymer) and 0.9 mL ethanol) onto fluorine-doped tin oxide glass, which was then dried in a vacuum oven. Aqueous Na_2SO_4(0.5 mol/L) solution was used as an electrolyte for the transient photocurrent response test, the electrochemical impedance test and the Mott-Schottky curve test. For the EIS experiment, the frequency range was from 0.1 kHz to 100.0 kHz. Mott-Schottky curve was obtained at 1.0 kHz frequency.

2 Results and Discussion

2.1 Structure, morphology and composition analyses

XRD characterization results of CN, N-CN and N-CN-$CoSe_x$-3 are shown in Fig. 1. The peaks at 13.1° and 27.2° for CN are attributed to the in-plane stacking of CN and the interlayer stacking of the aromatic ring structure, respectively. N-CN also has similar peak positions, indicating that nitrogen doping does not change the crystal structure of CN. Peaks of cobalt selenide were not observed for N-CN-$CoSe_x$-3, indicating that cobalt selenide may be in an amorphous form or that the content of $CoSe_x$ in N-CN-$CoSe_x$-3 is fairly low. However, since the surface of the N-CN is covered by $CoSe_x$, the peak at 27.2° for N-CN-$CoSe_x$-3 is weaker compared to that of CN and N-CN.

Figure 2 shows the morphology and the microstructure of N-CN-$CoSe_x$-3 which are characterized by TEM. It can be observed that irregular small black dots are scattered on N-CN, which are $CoSe_x$ particles. In the elemental mappings(Fig. 3), four elements (C, N, Co and Se) are presented in N-CN-$CoSe_x$-3, indicating that $CoSe_x$ is successfully loaded on N-CN. No lattice fringe of cobalt sulfide was observed in the high resolution TEM (Fig. 2), illustrating the amorphous property of cobalt sulfide obtained from photodeposition, which matched well with the result of XRD. The molar fraction of each element in N-CN-$CoSe_x$-3 measured by EDX is shown in Table 2, and it is demonstrated that the molar ratio of Co to Se is 1∶1.33 in N-CN-$CoSe_x$-3.

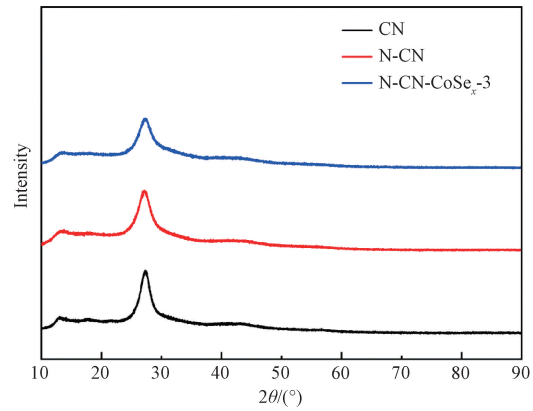

Fig. 1 XRD patterns of CN, N-CN and N-CN-$CoSe_x$-3

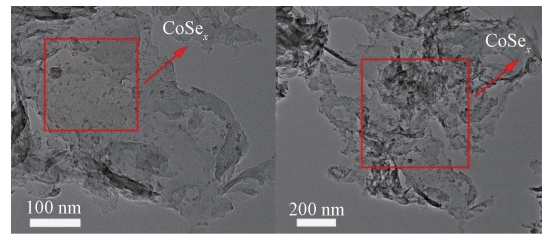

Fig. 2 TEM images of N-CN-$CoSe_x$-3

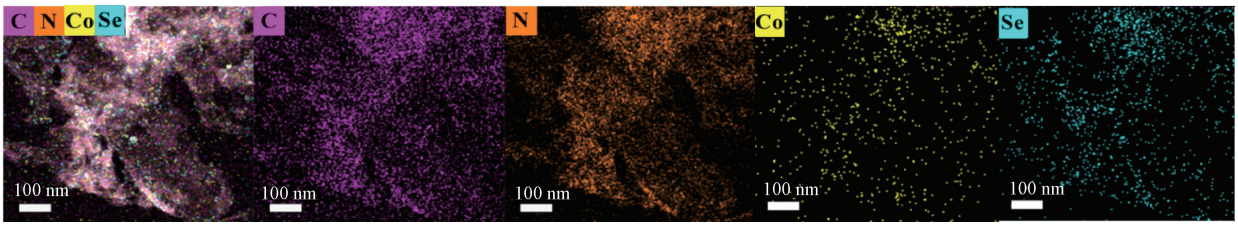

Fig. 3 Elemental mappings of N-CN-$CoSe_x$-3

Table 2 EDX results of N-CN-$CoSe_x$-3

Element	Molar fraction/%
C	42.11
N	57.26
Co	0.27
Se	0.36

The elemental composition and valence states of N-CN-$CoSe_x$-3 were characterized by XPS (Fig. 4). In the C1s spectrum (Fig. 4(a)), the peaks at 284.9 eV and 288.4 eV are attributed to N-CN and sp^2 hybridized carbon in the triazine ring, respectively[40-41]. In the N1s spectrum (Fig. 4(b)), the peak at 398.7 eV corresponds to the nitrogen in the C═N—C[42] and the peaks at 399.4 eV and 400.4 eV are attributed to the tertiary nitrogen N—$(C)_3$ and the nitrogen in C—N—H, respectively[43-44]. Notably, the peak at 401.2 eV corresponds to the graphite N, indicating the successful doping of nitrogen into CN[45]. In addition, the peak at 404.5 eV is caused by charge effects. In the Se3d spectrum (Fig. 4(c)), the binding energy at 51.8 eV and 57.6 eV are attributed to Se^{2-}[46]. As shown in Fig. 4(d), the peaks at 781.2 eV and 796.6 eV correspond to $2p_{3/2}$ and $2p_{1/2}$ of Co^{2+}, respectively, while the peaks at 785.9 eV and 803.5 eV belong to the satellite peaks of Co^{2+}[47].

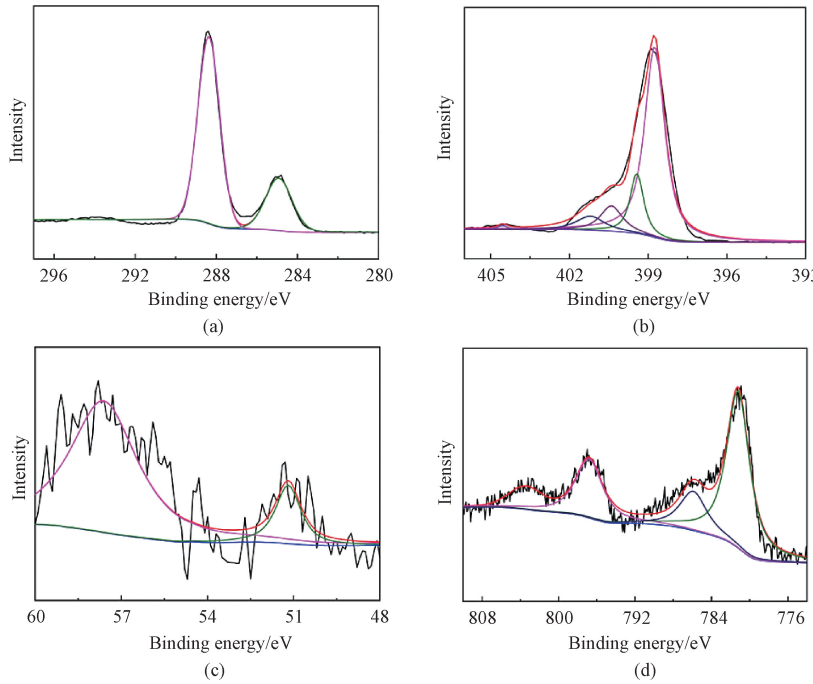

Fig. 4 High resolution XPS spectra: (a) C1s; (b) N1s; (c) Se3d; (d) Co2p

2.2 Optical properties and band structure analyses

As shown in Fig. 5(a), the light absorption exhibits a significant red shift after nitrogen-doping. After loading $CoSe_x$, N-CN-$CoSe_x$-3 shows a better light absorption ability. Besides, the stronger the light absorption ability of the catalyst, the more photogenerated electrons are generated to participate in the photocatalytic hydrogen production reaction, so N-CN-$CoSe_x$-3 has better performance in photocatalytic water splitting. Based on the UV-Vis diffuse reflection spectra, the band gap E_g of the semiconductor can be calculated according to

$$\alpha h\nu = A(h\upsilon - E_g)^{n/2}, \quad (1)$$

where α, υ, h and A are the absorption coefficient, the frequency, the Planck constant and the constant, respectively. As shown in Fig. 5(b), the band gaps of CN, N-CN and N-CN-$CoSe_x$-3 are 2.74 eV, 2.56 eV and 2.25 eV, respectively.

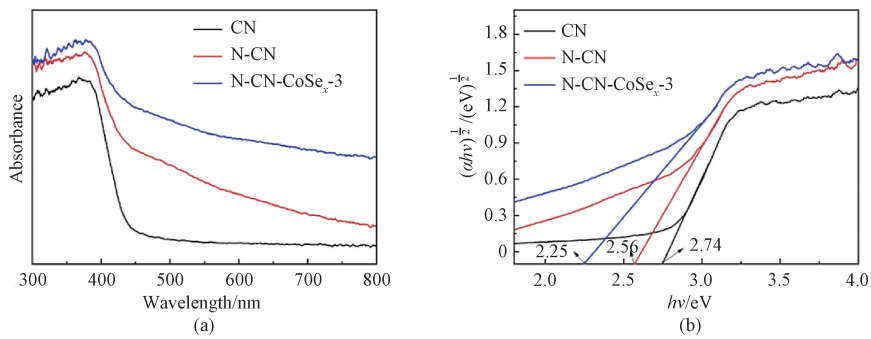

Fig. 5 Optical properties of CN, N-CN and N-CN-$CoSe_x$-3: (a) UV-Vis diffuse reflection spectra; (b) Tauc plots

2.3 Photocatalytic performance

The photocatalytic hydrogen production performance of CN, N-CN and N-CN-$CoSe_x$-3 were investigated under visible light irradiation. As shown in Fig. 6(a), the photocatalytic hydrogen production activities of CN and N-CN are both poor. The photocatalytic hydrogen production activity was significantly enhanced by loading $CoSe_x$ on N-CN. In addition, with the increase of co-catalyst loading, the photocatalytic hydrogen production activity of N-CN-$CoSe_x$-3 can reach 1 140 $\mu mol \cdot g^{-1} \cdot h^{-1}$, which is 285 times higher than that of CN. With further increasing the loading of $CoSe_x$, the photocatalytic hydrogen production performance decreases, which is because the excessive co-catalyst could affect the light absorption of N-CN and also the excessive $CoSe_x$ may become the recombination centers for photogenerated electrons and holes. In contrast, the photocatalytic hydrogen production activity of CN-$CoSe_x$-3 is only 410 $\mu mol \cdot g^{-1} \cdot h^{-1}$.

Besides, the photocatalytic hydrogen production activity of N-CN-$CoSe_x$-3 does not decrease significantly within four cycles, indicating that the composite catalyst has good cycling stability (Fig. 6(b)).

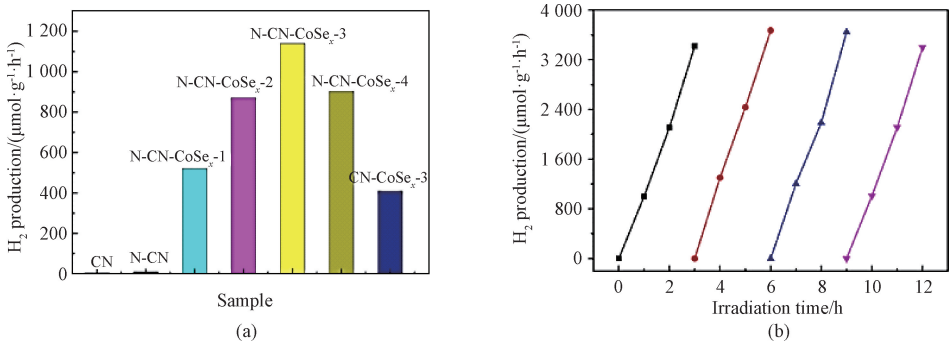

Fig. 6 Photocatalytic performance: (a) photocatalytic hydrogen production activity of different samples; (b) photocatalytic hydrogen production cycles of N-CN-$CoSe_x$-3

2.4 Photoelectrochemical properties

Photoluminescence (PL) spectra were examined and the results proved that nitrogen-doping and loading $CoSe_x$ could influence the photogenerated carrier separation efficiency. The stronger the fluorescence intensity, the quicker the photogenerated carriers are recombined. In the PL spectrum (Fig. 7(a)), compared with CN, the fluorescence intensity of N-CN is lower, indicating that nitrogen doping can reduce the photogenerated electron-hole recombination rate of CN. After loading $CoSe_x$, the fluorescence intensity of N-CN-$CoSe_x$-3 is further decreased, implying that loading $CoSe_x$ further inhibits the photogenerated electron-hole recombination, which is consistent with the photocatalytic hydrogen production activities of CN, N-CN and N-CN-$CoSe_x$-3. The separation and transfer of photogenerated electrons and holes can also be characterized by the *I-t* curves and electrochemical impedance spectra. The smaller the arc radius is in the electrochemical impedance spectra, the faster the charge transfer is. As shown in Fig. 7(b), compared with CN and N-CN, the radius of N-CN-$CoSe_x$-3 is the smallest, indicating that the charge transfer of the catalyst is faster with the loading of $CoSe_x$. In Fig. 7(c), the photocurrent intensity of N-CN-$CoSe_x$-3 is higher than that of CN and N-CN, illustrating that the $CoSe_x$ loaded N-CN has better separation of photogenerated electrons and holes.

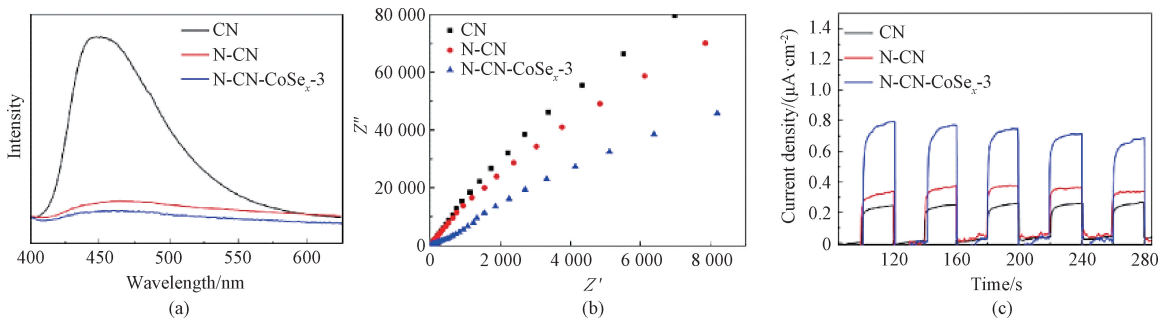

Fig. 7 Photoelectrochemical tests of CN, N-CN and N-CN-$CoSe_x$-3: (a) PL spectra; (b) electrochemical impedance spectra; (c) *I-t* curves

2.5 Reaction mechanism of photocatalytic hydrogen production

The mechanism for photocatalytic hydrogen production of N-CN-$CoSe_x$-3 was proposed based on the above results and analysis, as shown in Fig. 8. Under light excitation, N-CN generates photogenerated electrons (e^-) and holes (h^+), and the photogenerated e^- leap from the valence band (VB) of N-CN to the conduction band (CB). Then, the electrons transfer to the surface of $CoSe_x$ for the reduction of H^+ to produce hydrogen, while the holes on the VB are quenched by TEOA. Introducing $CoSe_x$ accelerates the photogenerated electron transfer and offers more active sites, thus enhancing the performance of photocatalytic hydrogen production.

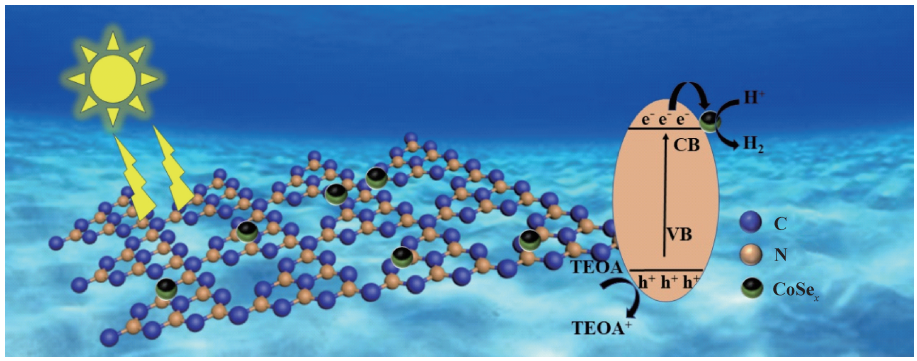

Fig. 8 Mechanism of photocatalytic reaction of N-CN-$CoSe_x$-3

3 Conclusions

Cobalt selenide-loaded nitrogen-doping graphite carbon nitride composites were prepared by the photochemical synthesis method. The highest photocatalytic hydrogen production activity was observed for N-CN-$CoSe_x$-3, which was 285 times higher than that of CN. Photoelectrochemical tests confirmed that the light adsorption capability and the separation and transfer of photogenerated electrons and holes were improved by nitrogen-doping and the loading of $CoSe_x$, which contributed to the enhanced hydrogen production activity. This study offers a new insight into the synthesis of composite photocatalysts by loading transition metal selenides as co-catalysts by photochemical synthesis.

References

[1] BOUMERIAME H, DA SILVA E S, CHEREVAN A S, et al. Layered double hydroxide (LDH)-based materials: a mini-review on strategies to improve the performance for photocatalytic water splitting [J]. *Journal of Energy Chemistry*, 2022, 64: 406-431.

[2] ZHAO Y J, LI Y, SUN L D. Recent advances in photocatalytic decomposition of water and pollutants for sustainable application [J]. *Chemosphere*, 2021, 276: 130201.

[3] SHARMA S, BASU S, SHETTI N P, et al. Waste-to-energy nexus: a sustainable development [J]. *Environmental Pollution*, 2020, 267: 115501.

[4] YUAN W W, HUANG Y G, MENG W D. Visible-light photoredox-catalyzed three-component tandem trifluoromethylation/gemdifluoroallylation of alkenes [J]. *Journal of Donghua University (English Edition)*, 2024, 41(1): 57-71.

[5] LI F H, LIU Y H, MAO B D, et al. Carbon-dots-mediated highly efficient hole transfer in I-III-VI quantum dots for photocatalytic hydrogen production [J]. *Applied Catalysis B: Environmental*, 2021, 292: 120154.

[6] ELBESHBISHY E, DHAR B R, NAKHLA G, et al. A critical review on inhibition of dark biohydrogen fermentation [J]. *Renewable & Sustainable Energy Reviews*, 2017, 79: 656-668.

[7] TURHAL S, TURANBAEV M, ARGUN H. Hydrogen production from melon and watermelon mixture by dark fermentation [J]. *International Journal of Hydrogen Energy*, 2019, 44(34): 18811-18817.

[8] HE F, CHEN G, ZHOU Y S, et al. The facile synthesis of mesoporous g-C_3N_4 with highly enhanced photocatalytic H_2 evolution performance [J]. *Chemical Communications*, 2015, 51(90): 16244-16246.

[9] WADJEAM P, REUNGSANG A, IMAI T, et al. Co-digestion of cassava starch wastewater with buffalo dung for bio-hydrogen production [J]. *International Journal of Hydrogen Energy*, 2019, 44(29): 14694-14706.

[10] WANG B, ZHANG Q, HE J Q, et al. Co-catalyst-free large ZnO single crystal for high-efficiency piezocatalytic hydrogen evolution from pure water [J]. *Journal of Energy Chemistry*, 2022, 65(2): 304-311.

[11] LIU Y, SUN Y P, XU J, et al. A Z-scheme heterostructure constructed from ZnS nanospheres and Ni(OH)$_2$ nanosheets to enhance the photocatalytic hydrogen evolution [J]. *New Journal of Chemistry*, 2021, 45(17): 7781-7791.

[12] FUJISHIMA A, HONDA K. Electrochemical photolysis of water at a semiconductor electrode [J]. *Nature*, 1972, 238: 37-38.

[13] ZHU Y K, LI J Z, DONG C L, et al. Red phosphorus decorated and doped TiO_2 nanofibers for efficient photocatalytic hydrogen evolution from pure water [J]. *Applied Catalysis B: Environmental*, 2019, 255: 117764.

[14] ZHANG R G, GONG K W, DU F Y, et al. Highly efficient thiomolybdate $Mo_2S_{12}^{2-}$ nanocluster cocatalyst decorated on TiO_2 to boost

photocatalytic hydrogen evolution [J]. *International Journal of Hydrogen Energy*, 2022, 47(45): 19570-19579.

[15] AHMAD I, SHUKRULLAH S, NAZ M Y, et al. Construction of Ag-modified ZnO-CeO_2 2D-1D S-scheme heterojunction photocatalyst with phenomenal photocatalytic performance for H_2 evolution [J]. *Materials Science in Semiconductor Processing*, 2023, 159: 107392.

[16] QIN H F, ZUO Y H, JIN J T, et al. ZnO nanorod arrays grown on g-C_3N_4 micro-sheets for enhanced visible light photocatalytic H_2 evolution [J]. *RSC Advances*, 2019, 9(42): 24483-24488.

[17] LI S S, WANG L, LI Y D, et al. Novel photocatalyst incorporating Ni-Co layered double hydroxides with P-doped CdS for enhancing photocatalytic activity towards hydrogen evolution [J]. *Applied Catalysis B: Environmental*, 2019, 254: 145-155.

[18] LEI Y G, HOU J H, WANG F, et al. Boosting the catalytic performance of MoS_x cocatalysts over CdS nanoparticles for photocatalytic H_2 evolution by Co doping via a facile photochemical route[J]. *Applied Surface Science*, 2017, 420: 456-464.

[19] DU C, ZHANG Q, LIN Z Y, et al. Half-unit-cell $ZnIn_2S_4$ monolayer with sulfur vacancies for photocatalytic hydrogen evolution [J]. *Applied Catalysis B: Environmental*, 2019, 248: 193-201.

[20] LI Z J, WANG X H, TIAN W L, et al. CoNi bimetal cocatalyst modifying a hierarchical $ZnIn_2S_4$ nanosheet-based microsphere noble-metal-free photocatalyst for efficient visible-light-driven photocatalytic hydrogen production [J]. *ACS Sustainable Chemistry & Engineering*, 2019, 7(24): 20190-20201.

[21] SHE X J, WU J J, ZHONG J, et al. Oxygenated monolayer carbon nitride for excellent photocatalytic hydrogen evolution and external quantum efficiency[J]. *Nano Energy*, 2016, 27: 138-146.

[22] LI C H, LIANG Y L, LU Z F, et al. $NiCo_2S_4$ decorated g-C_3N_4 nanosheets for enhanced photocatalytic hydrogen evolution[J]. *Journal of Nanoparticle Research*, 2020, 22(2): 41.

[23] WU M, YAN J M, ZHANG X W, et al. Ag_2O modified g-C_3N_4 for highly efficient photocatalytic hydrogen generation under visible light irradiation [J]. *Journal of Materials Chemistry A*, 2015, 3(30): 15710-15714.

[24] MA W Y, ZHENG D W, XIAN Y X, et al. Efficient hydrogen evolution under visible light by bimetallic phosphide NiCoP combined with g-C_3N_4/CdS S-scheme heterojunction [J]. *Chemcatchem*, 2021, 13(20): 4403-4410.

[25] HU L J, YANG H L, WANG S H, et al. MOF-derived hexagonal In_2O_3 microrods decorated with g-C_3N_4 ultrathin nanosheets for efficient photocatalytic hydrogen production [J]. *Journal of Materials Chemistry C*, 2021, 9(16): 5343-5348.

[26] DENG P H, HONG W S, CHENG Z W, et al. Facile fabrication of nickel/porous g-C_3N_4 by using carbon dot as template for enhanced photocatalytic hydrogen production [J]. *International Journal of Hydrogen Energy*, 2020, 45(58): 33543-33551.

[27] GUO F, WANG L J, SUN H R, et al. High-efficiency photocatalytic water splitting by a N-doped porous g-C_3N_4 nanosheet polymer photocatalyst derived from urea and *N*, *N*-dimethylformamide [J]. *Inorganic Chemistry Frontiers*, 2020, 7(8): 1770-1779.

[28] LIU Q Q, SHEN J Y, YU X H, et al. Unveiling the origin of boosted photocatalytic hydrogen evolution in simultaneously (S, P, O)-codoped and exfoliated ultrathin g-C_3N_4 nanosheets [J]. *Applied Catalysis B: Environmental*, 2019, 248: 84-94.

[29] WANG R Y, WANG X Y, LI X C, et al. Facile one-step synthesis of porous graphene-like g-C_3N_4 rich in nitrogen vacancies for enhanced H_2 production from photocatalytic aqueous-phase reforming of methanol[J]. *International Journal of Hydrogen Energy*, 2021, 46(1): 197-208.

[30] ZHAO H, DONG Y M, JIANG P P, et al. In situ light-assisted preparation of MoS_2 on graphitic C_3N_4 nanosheets for enhanced photocatalytic H_2 production from water[J]. *Journal of Materials Chemistry A*, 2015, 3(14): 7375-7381.

[31] LI D D, DONG Y M, WANG G L, et al. Controllable photochemical synthesis of amorphous Ni(OH)$_2$ as hydrogen production cocatalyst using inorganic phosphorous acid as sacrificial agent [J]. *Chinese Journal of Catalysis*, 2020, 41(5): 889-897.

[32] LIU Y H, HUANG H, CAO W J, et al. Advances in carbon dots: from the perspective of traditional quantum dots[J]. *Materials Chemistry Frontiers*, 2020, 4(6): 1586-1613.

[33] XU Y Q, DU C, ZHOU C, et al. Ternary noble-metal-free heterostructured NiS-CuS-C_3N_4 with near-infrared response for enhanced photocatalytic hydrogen evolution [J]. *International Journal of Hydrogen Energy*, 2020, 45(7): 4084-4094.

[34] LIANG Z Q, SUN B T, XU X S, et al. Metallic 1T-phase MoS_2 quantum dots/g-C_3N_4 heterojunctions for enhanced photocatalytic hydrogen evolution [J]. *Nanoscale*, 2019, 11(25): 12266-12274.

[35] PATNAIK S, SAHOO D P, PARIDA K. Recent

advances in anion doped g-C_3N_4 photocatalysts: a review[J]. *Carbon*, 2021, 172: 682-711.
[36] HASIJA V, RAIZADA P, SUDHAIK A, et al. Recent advances in noble metal free doped graphitic carbon nitride based nanohybrids for photocatalysis of organic contaminants in water: a review[J]. *Applied Materials Today*, 2019, 15: 494-524.
[37] WANG M, CHENG J J, WANG X F, et al. Sulfur-mediated photodeposition synthesis of NiS cocatalyst for boosting H_2 evolution performance of g-C_3N_4 photocatalyst[J]. *Chinese Journal of Catalysis*, 2021, 42(1): 37-45.
[38] GAO D D, WU X H, WANG P, et al. Selenium-enriched amorphous $NiSe_{1+x}$ nanoclusters as a highly efficient cocatalyst for photocatalytic H_2 evolution [J]. *Chemical Engineering Journal*, 2021, 408: 127230.
[39] YU H G, XU J C, GAO D D, et al. Triethanolamine-mediated photodeposition formation of amorphous Ni-P alloy for improved H_2-evolution activity of g-C_3N_4 [J]. *Science China Materials*, 2020, 63(11): 2215-2227.
[40] SHEN Q, JIANG P J, HE H C, et al. Designing g-C_3N_4/N-rich carbon fiber composites for high-performance potassium-ion hybrid capacitors[J]. *Energy & Environmental Materials*, 2021, 4(4): 638-645.
[41] JIN C Y, WANG M, LI Z L, et al. Two dimensional Co_3O_4/g-C_3N_4 Z-scheme heterojunction: mechanism insight into enhanced peroxymonosulfate-mediated visible light photocatalytic performance [J]. *Chemical Engineering Journal*, 2020, 398: 125569.
[42] ZHANG J Y, MEI J Y, YI S S, et al. Constructing of Z-scheme 3D g-C_3N_4-ZnO @ graphene aerogel heterojunctions for high-efficient adsorption and photodegradation of organic pollutants [J]. *Applied Surface Science*, 2019, 492: 808-817.
[43] ZHU D D, ZHOU Q X. Nitrogen doped g-C_3N_4 with the extremely narrow band gap for excellent photocatalytic activities under visible light[J]. *Applied Catalysis B: Environmental*, 2021, 281: 119474.
[44] XIAO M S, ZHANG Z H, TIAN Y P, et al. Co-Fe-Se ultrathin nanosheet-fabricated microspheres for efficient electrocatalysis of hydrogen evolution [J]. *Journal of Applied Electrochemistry*, 2017, 47(3): 361-367.
[45] SHI Q, LIU Q, ZHENG Y P, et al. Controllable construction of bifunctional Co_xP @ N, P-doped carbon electrocatalysts for rechargeable zinc-air batteries [J]. *Energy & Environmental Materials*, 2022, 5(2): 515-523.
[46] KIM E H, REDDY D A, LEE H, et al. Hollow $CoSe_2$ nanocages derived from metal-organic frameworks as efficient non-precious metal co-catalysts for photocatalytic hydrogen production [J]. *Catalysis Science & Technology*, 2019, 9(17): 4702-4710.
[47] DU S W, LIN X, LI C H, et al. $CoSe_2$ modified Se-decorated CdS nanowire Schottky heterojunctions for highly efficient photocatalytic hydrogen evolution [J]. *Chemical Engineering Journal*, 2020, 389: 124431.

N 掺杂和光化学合成 $CoSe_x$ 助催化剂改性石墨相氮化碳以提高其光催化产氢性能

刘思伟[1,2], 郗传俊[1,2], 张琳萍[1,2], 宣为民[1,2], 侯 煜[1,2*]
1. 东华大学 化学与化工学院, 上海 201620
2. 东华大学 生态纺织教育部重点实验室, 上海 201620

摘 要: 开发一种高效的产氢光催化剂对于将太阳能转化为氢能至关重要。该研究将氮掺杂石墨相氮化碳(CN)与光化学合成得到的助催化剂 $CoSe_x$ 相结合, 通过原位合成制备了一种高效的光催化产氢材料。该材料的最佳光催化性能较 CN 提高 285 倍。光电化学试验表明, 氮掺杂和引入 $CoSe_x$ 可以有效促进光生电荷载流子的分离, 从而提高 CN 的产氢活性。该工作为利用光化学沉积方法制备新型光催化剂提供了新的视角。

关键词: 光催化剂; $CoSe_x$; 助催化剂; 产氢; 氮掺杂